Environmental Science and Pollution Research
https://doi.org/10.1007/s11356-022-20488-4

RESEARCH ARTICLE

Polishing of painting process effluents through adsorption with biochar from winemaking residues

Fernando L. Carvalho[1] · Diana Pinto[2] · Rejiane R. Schio[1] · Jaqueline P. dos Santos[1] · Felipe Ketzer[3] · Luis F. O. Silva[2] · Guilherme L. Dotto[1]

Received: 28 January 2022 / Accepted: 24 April 2022
© The Author(s), under exclusive licence to Springer-Verlag GmbH Germany, part of Springer Nature 2022

Abstract
A real industrial effluent from the pre-treatment and painting processes was polished through adsorption using alternative biochar derived from grape pomace wastes. The biochar was produced in a pilot-scale plant from composted grape pomace. Biochar showed an equilibrium between acidic and basic groups on the surface. The presence of irregular cavities in the structure and mesopores was confirmed by analyzing N_2 physisorption and SEM. Concerning the effluent, Ni and Zn were the main problematic elements. The adsorption isotherms and kinetics of Ni and Zn from the effluent using the biochar could be represented by the Henry, pseudo-first-order, and pseudo-second-order models, respectively. Adsorption equilibrium was reached within 60 min for Ni and Zn present in the real effluent. Besides, the adsorption process was endothermic, favorable, and spontaneous. These results demonstrate that Zn and Ni metals were successfully removed from the industrial effluent, presenting final concentration values within the limit of legislation for effluent disposal in agricultural soil.

Keywords Grape pomace biochar · Effluent · Metal removal · Adsorption

Introduction

Industrial wastewater can contain a variety of organic and inorganic pollutants, and if it reaches the water body, it can seriously alter its characteristics. Inorganic pollutants include heavy metals, phosphate, nitrate, sulfate, etc. Among the heavy metals, As, Cu, Cd, Cr, Ni, Zn, Pb, Hg, and Mn are the main pollutants to freshwater reserves due to their toxic, non-biodegradable, persistent nature, biomagnification, and bioaccumulation in the food chain (Bilal et al. 2013; Peng and Bartzas 2021). In industrial painting processes (painting by electrophoresis), we find some of the metals mentioned above in their composition, especially in the automotive field. For the industrial painting process to be effective, replacing and removing water from the system are necessary. The treatment of effluents is then essential for this water to return to the environment (Yang et al. 2021). In wastewater treatment, chemical precipitation is one of the most commonly used conventional processes for removing heavy metals (Oncel et al. 2013). This technique is more accessible and suitable for treating polluted water with high concentrations of heavy metals and is not suitable for low concentrations of metal ions (Gope and Saha 2021). The wastewater that was the object of the study underwent chemical precipitation to remove metals. However, it did not meet the standards required by current legislation.

From the perspective of circular economy and green development, adsorption technology can be a choice to remove toxic metal ions in wastewater (Zhou et al. 2016). According to Rathi and Kumar (2021), adsorption is advantageous over other effluent treatment methods due to its low-cost, simple design, easy use, and resistance to harmful substances. The adsorbents applied in the different branches can be natural

Responsible Editor: Zhihong Xu

✉ Luis F. O. Silva
lsilva8@cuc.edu.co

✉ Guilherme L. Dotto
guilherme_dotto@yahoo.com.br

[1] Research Group On Adsorptive and Catalytic Process Engineering (ENGEPAC), Federal University of Santa Maria, Av. Roraima, 1000-7, Santa Maria, RS 97105–900, Brazil

[2] Department of Civil and Environmental, Universidad de La Costa, CUC, Calle 58 # 55–66, Barranquilla, Atlántico, Colombia

[3] Federal Institute of Education, Science and Technology Farroupilha, Erechim Avenue, Panambi, RS 860, 98280-000, Brazil

Published online: 02 May 2022

(organic and inorganic) or synthetic. Most are specially manufactured materials, such as activated carbon, and others are naturally available, such as zeolites, but some adsorbents usually have extensive treatment to achieve their most effective form. Examples include activated alumina, activated carbon, silica, zeolites, clays, and polymeric adsorbents (Tareq et al. 2019). As the adsorbents represent 70% of the cost in adsorption, the search for alternative materials has gained prominence in the current scenario (Dotto and McKay 2020). According to Cao et al. (2011), biochar is quite similar to activated carbon concerning mutual production via pyrolysis, with medium and high surface areas. However, biochar is generally not activated or treated (Cao and Harris 2010; Ahmad et al. 2012). Biochar has attracted worldwide attention as a useful, low-cost, and ecologically correct adsorbent for the remediation of various pollutants due to its large surface area, high adsorption capacity, micro-mesoporosity, and ion exchange capacity (Tareq et al. 2019). Studies by Li et al. (2019), Roy and Bharadvaja (2021), and Vilvanathan and Shanthakumar (2015) described an effective removal of metals from water using biochar originating from different organic wastes. However, the great majority of the works in this field are about the preparation of biochar in lab-scale to treat synthetic effluents (water + metal). In our case, the biochar was developed on a pilot-scale, and the treatment was performed in a real effluent from the pre-treatment and painting processes.

The objectives of this work were the preparation and characterization of biochar originating from organic by-products of the wine industry in a pilot-scale pyrolysis unit, the evaluation of the adsorption operation using this biochar for the polishment of a painting process effluent. For industrial application, the effluent must meet the conditions of the current operating license, which limits the release of pollutants into the agricultural soil to 0.2 mg L^{-1} for Ni and 2.0 mg L^{-1} to Zn. Compliance with the conditions is based on the National Council for the Environment (CONAMA) No. 420 of 2009, CONAMA No. 357 of 2005, and the State Council for the Environment (CONSEMA) No. 355 of 2017.

Materials and methods

Materials

The industrial effluent was obtained from the wastewater treatment plant of a local company, originating from the pre-treatment and painting process. The effluent generated in the rinsing steps, coming from water obtained from artesian wells belonging to the company, is released onto agricultural soil and carries a heavy metal residue (Ni, Fe, Mn, and Zn) which needs to meet the parameters and standards of current legislation. A producer from the Serra Gaúcha provided the Chardonnay grape pomace sample (the Rio Grande do Sul, Brazil, in the 2017 harvest), which was composted for 3 years through the Beifiur® composting process. This grape composted waste (GCW) was used to produce the biochar.

Biochar from Serra Gaúcha (BSG) preparation

The pyrolysis was carried out in a cubic oven (Beifiur Ltda) with temperature and product flow control. About 5 kg of the biomass (GCW) was fed into the reactor and heated from atmospheric temperature (20 °C) to the respective pyrolysis temperature (550 °C) at a heating rate around 1 °C min^{-1}. The residence time was 24 h to allow sufficient time for complete pyrolysis under oxygen-limited conditions. The samples were then allowed to cool slowly to room temperature in the pyrolyzer. The Serra Gaúcha Biochar (BSG) was conditioned to an acid/base pre-treatment before analysis. The following steps carried out the pre-treatment: acid treatment (H_2SO_4, 0.1 mol L^{-1}), washing the sample with distilled water (1:2), basic treatment (NaOH, 0.1 mol L^{-1}), washing the samples (neutralizing the pH), drying (24 h at room temperature and 48 h in an oven at 60 °C), and sieving (1 mm).

BSG characterization

See supplementary material S1.

Polishing the effluent using adsorption experiments

All adsorption experiments were conducted in batch at 200 rpm in a thermostated shaker (Marconi, MA 093, Brazil). First, the effect of the adsorbent dosage of the BSG adsorbent on the adsorption of metals was investigated. Adsorbent dosage was varied from 0.25 to 10 g L^{-1}, pH 8 (natural effluent pH), at 298 K for 2 h. The study of the effect of pH was verified from 4 to 8 (NaOH and HCl (0.1 mol L^{-1})). The experiments were carried out with the best adsorbent dosage, at 298 K for 2 h. Afterward, kinetic curves were quantified (contact time from 0 to 140 min), using the natural effluent pH, the best adsorbent dosage, and a solution volume of 50 mL, at 298 K. Finally, equilibrium curves were obtained at different temperatures (298, 308, 318, and 328 K), varying the adsorbent dosage from 0.25 to 10 g L^{-1}, since the initial concentration of the real effluent is fixed. The experiments were carried out at the natural pH of the effluent with the best BSG dosage for 6 h. After each adsorption test, the concentrations of metals remaining in the liquid phase were analyzed by flame atomic absorption spectroscopy in Agilent Technologies equipment (model 240FS A.A.). The tests were carried out in triplicate. Polishing treatment was evaluated according to supplementary material S2.

Kinetic, equilibrium, and thermodynamics of the polishing

The kinetic models of pseudo-first-order (PFO) (Eq. 1) and pseudo-second-order (PSO) (Eq. 2) were applied to represent the kinetic curves (Dotto et al. 2017):

$$q_t = q_1\left(1 - \exp\left(-k_1 t\right)\right) \tag{1}$$

$$q_t = \frac{1}{\left(\frac{1}{k_2 q_2^2}\right) + \left(\frac{t}{q_2}\right)} \tag{2}$$

where k_1 (min^{-1}) and k_2 (g mg^{-1} min^{-1}) are the rate constants of PFO and PSO models and q_1 and q_2 (mg g^{-1}) are the theoretical values for the adsorption capacity.

The equilibrium of the adsorption process was evaluated based on the Henry model (Eq. 3), which is based on the proposal that the adsorption capacity is directly proportional to the solute concentration in an aqueous medium (Piccin et al. 2017):

$$q_e = k_H C_e \tag{3}$$

where k_H is the Henry constant (L g^{-1}).

The thermodynamic parameter variation of the standard Gibbs free energy (ΔG^0, kJ mol^{-1}), standard entropy variation (ΔS^0, kJ mol^{-1} K^{-1}), and standard enthalpy variation (ΔH^0, kJ mol^{-1}) were estimated according to the methodology proposed by Lima et al. (2019) through Eqs. 4, 5, and 6:

$$\Delta G^0 = -RT\ln\left(K_e\right) \tag{4}$$

$$\Delta G^0 = \Delta H^0 - T\Delta S^0 \tag{5}$$

$$\ln\left(K_e\right) = \frac{\Delta S^0}{R} - \frac{\Delta H^0}{RT} \tag{6}$$

where K_e is the thermodynamic equilibrium constant (dimensionless), R is the universal gas constant (8.31×10^{-3} kJ mol^{-1} K^{-1}), and T is the temperature (K). The K_e value was estimated from the Henry constant (k_H), each metal's molecular mass, and activity coefficients in the solution.

The fitting of the models and also the statistical evaluation of the estimated parameters was performed according to Piccin et al. (2017), Dotto et al. (2017), and Bonilla-Petriciolet et al. (2019).

Results and discussion

Characteristics of painting process effluent

Table 1 shows the characteristics of the industrial effluent before the polishing using adsorption. The treatment of industrial effluent from the present paint industry consists mainly of the E-coat process. Although the process is quite efficient for removing suspended material, the concentration of some heavy metals is still very high, and the final effluent is not suitable for disposal. Therefore, preliminary tests were carried out for the four heavy metals of interest (Ni, Fe, Mn, and Zn). These tests revealed that Fe (0.137 mg L^{-1}) and Mn (0.113 mg L^{-1}) (Table 1), in addition to being within the standards required for application in agricultural

Table 1 Characteristics of the real effluent from the pre-treatment and painting processes

Characteristics	February 2021	Mean 2020	Mean 2019	Mean 2018
Ca (mg L^{-1})	39.6	54.6	58.8	128.1
Conductivity (mS cm^{-1})	1.7	1.2	1.2	––
BOD (mg L^{-1})	3.0	9.3	10.5	11.6
COD (mg L^{-1})	10.1	26.6	30.0	35.8
Phenol (mg L^{-1})	0	0.003	0.010	0.040
Fe (mg L^{-1})	0.137	0.212	0.180	0.466
Total P (mg L^{-1})	0.260	1.145	2.483	1.244
Mg (mg L^{-1})	1.540	2.169	1.685	2.392
Mn (mg L^{-1})	0.113	0.138	0.180	0.356
Ni (mg L^{-1})	0.406	0.414	0.499	0.576
Ammonia nitrogen (mg L^{-1})	2.000	1.992	2.000	5.000
NTK (mg L^{-1})	4.42	3.74	4.21	5.26
Oil and grasses (mg L^{-1})	5.000	4.500	6.039	10.000
pH	7.98	7.47	6.62	––
Na (mg L^{-1})	280.0	177.3	183.6	191.1
Zn (mg L^{-1})	0.090	0.404	0.533	0.643

soil, also did not show significant lows after preliminary tests. Thus, subsequent studies were continued only with the metals Zn (0.09 mg L^{-1}) and Ni (0.406 mg L^{-1}) (Table 1), the latter having a concentration greater than that required by the regulatory agency. It should be highlighted that Ni has been a great problem for the industry since 2018. In this period, the final concentrations of Ni were always higher than 0.4 mg L^{-1}. The limit, in turn, is 0.2 mg L^{-1}.

BSG characteristics

The main functional groups of BSG are shown in the FTIR spectrum (Fig. 1). The BSG spectrum has much in common with those reported for lignocellulosic-based biochars (Casazza et al. 2016; Ferrari et al. 2019). The intense OH elongation bands at 3423.8 cm^{-1} and C–O around 1070 cm^{-1} are typical biochars (Sardella et al. 2015). The bands at 1608 and 1495 cm^{-1} were attributed to aromatic C–H bonds and C = C elongation bands, respectively, which are typical of aromatic molecules. Also related to bands at wavenumbers below 900 cm^{-1} attributed to C–H binding in aromatic structures (Anirudhan and Sreekumari 2011). The bands at 1074.4, 796.6, 780.2, and 460.0 cm^{-1} were attributed to the vibrations of asymmetric and symmetric elongation of Si–O–Si bonds, stretching vibration, $v_{asSi\text{-}OH}$, and bending vibration ($\delta_{Si\text{-}O\text{-}Si}$); similar results were found by Brezoiu et al. (2019) for red grape pomace.

Figure 2 shows the XRD patterns for the BSG. In the diffractogram, it is possible to observe an important low-intensity peak at the position $2\Theta = 21.7°$ which may be related to the residual crystallinity of the cellulose. Mulinari et al. (2009) reported that this peak ($2\theta = 22°$) was found in cellulose samples. Furthermore, the BSG showed an intense reflection at the peak $2\Theta = 26.54°$. This peak has been related to graphite structure, which is indicative of the stacking of some graphene-like layers on activated carbon (González-García 2018). Furthermore, a region with crystalline peaks between 20 and 26° (2θ) corresponds to crystalline Si, also verified by Pigatto et al. (2020) and Silva et al. (2021).

The SEM micrographs of biochar are shown at two magnifications (250 and 1000×) and presented in Fig. 3a and b. The biochar obtained showed an irregular surface of different shapes and sizes and a porous structure visible in images related to 1000× magnification. In addition, cavities and lumps, typical of activated carbon, can be seen in the material (Shao et al. 2012). The presence of irregular cavities in the adsorbent structure is favorable as they allow the penetration of adsorbate molecules (Lütke et al. 2019). The surface area, total pore volume, and mean pore size of

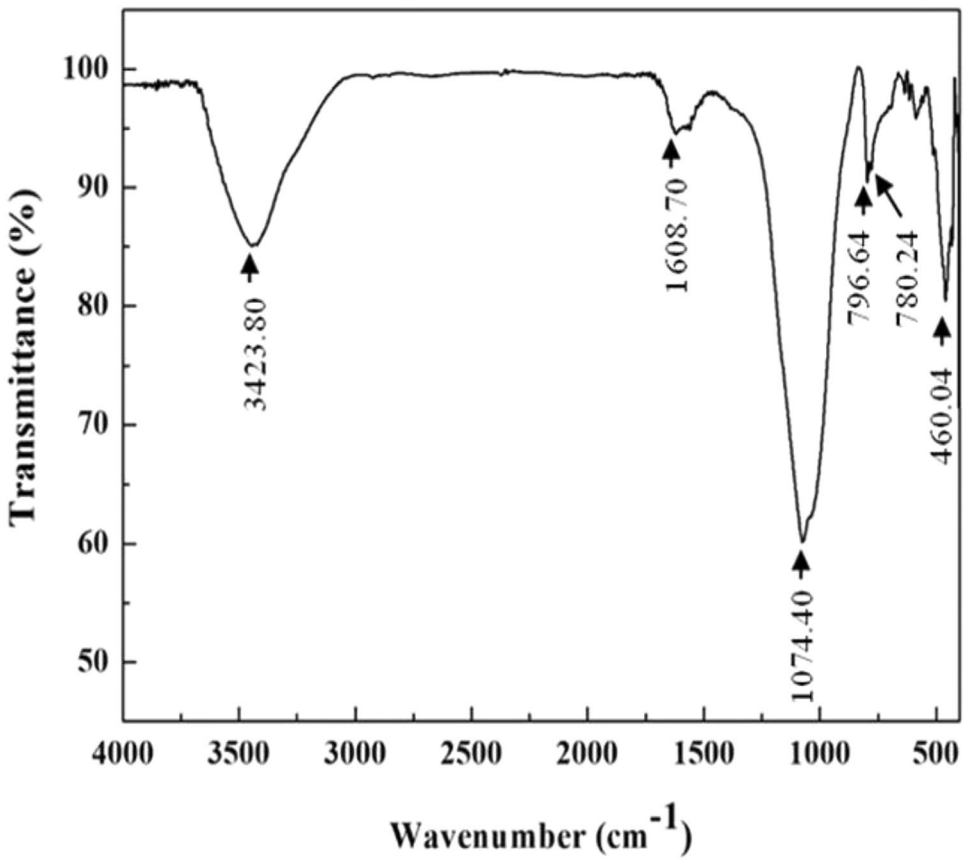

Fig. 1 FTIR vibrational spectrum of BSG

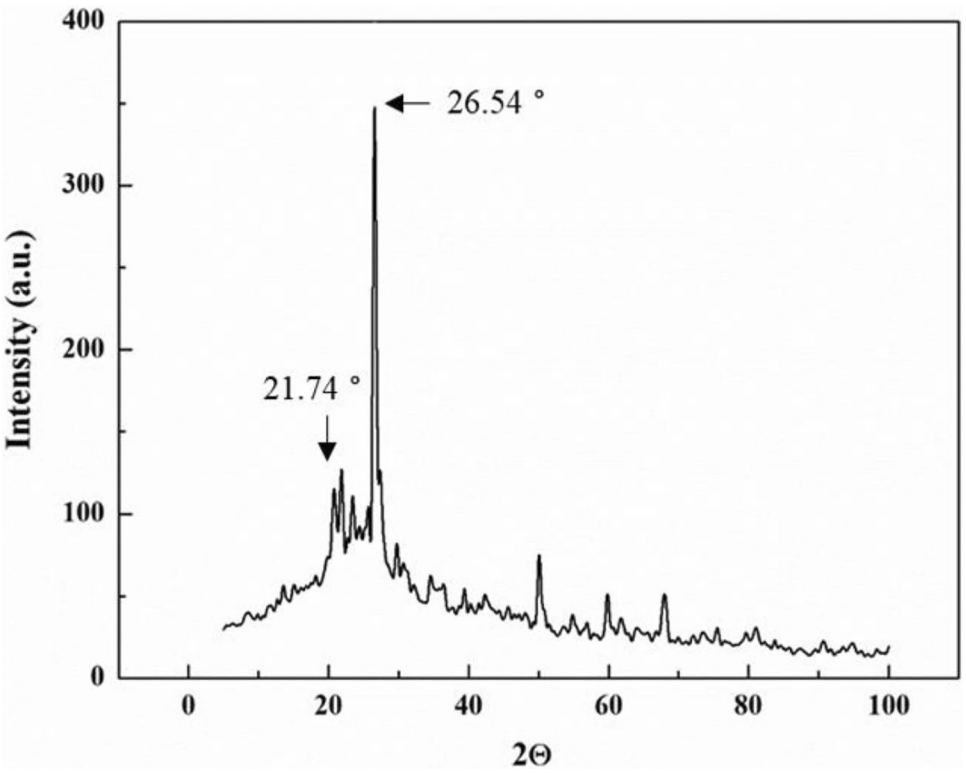

Fig. 2 XRD pattern of BSG

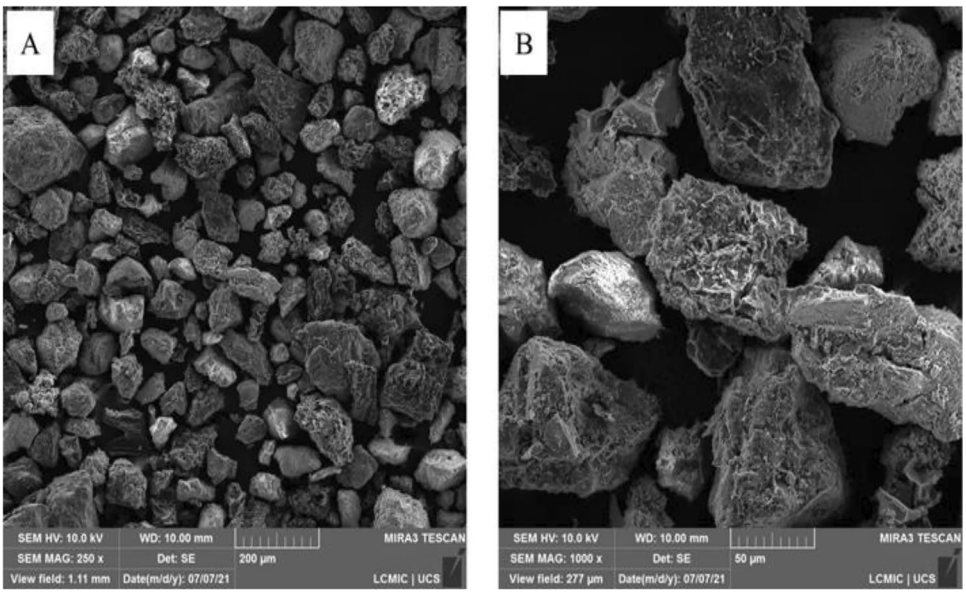

Fig. 3 SEM images of BSG: **a** × 250 and **b** × 1000

BSG were 7.84 m^2 g^{-1}, 0.017 cm^3 g^{-1}, and 3.7 nm, respectively. According to the IUPAC (Sing et al. 1985), BSG is mesoporous.

Boehm titrations determined activated carbons' surface basicity and acidity (Tang and Ahmad Zaini 2020). The concentration of total acid groups was 0.80 mmol L^{-1}, the carboxylic groups were 0.55 mmol L^{-1}, the lactone groups were 0.10 mmol L^{-1}, and the phenolic groups were 0.15 mmol L^{-1}. Acidity and basicity are related to acidic and basic groups available on the surface of activated carbon (Al−Lagtah et al. 2016). The BSG showed total basic groups on the sample surface of 0.80 mmol L^{-1}, demonstrating an equilibrium between acid and basic groups on the sample surface, which may be related to washes to neutralize the pH performed in the sample preparation.

The point of zero charge (pH_{PZC}) corresponds to the pH value where the net charge on the surface of the adsorbent is equal to zero. The pH value has the same positive and negative ions concentrations on the material's surface; thus, the pH_{PZC} provides information about the pH to adsorb anionic or cationic species (Dil et al. 2019). Furthermore, due to the relationship that the pH_{PZC} has with the acidic and basic functional groups present on the sample surface, it is possible to predict the nature of the surface of the adsorbent (Al−Lagtah et al. 2016). For example, the pH_{PZC} value for BSG was 7.05, which indicates a neutralized surface. This result corroborates the results found for the Boehm titration, confirming the neutral nature of the BSG surface.

The curve was divided into three main stages according to the TGA performed on the BSG sample (Fig. 4). In the first thermal event (22–130 °C), a mass loss of 3.1% is compatible with water volatilization (Rosa et al. 2017). In the second stage (130–375 °C), there is a mass loss of only 3.2%, which may be related to the water molecules that were trapped in the carbonaceous matrix; the final mass loss (15.0%) between temperatures of 375–776 °C is attributed to partial decomposition of the carbonaceous skeleton (Silva et al. 2021; Santos et al. 2015). Besides, it is of great importance to note that at 776 °C, the residual mass of the BSG sample was 79.7% of the initial mass, which demonstrates thermal stability.

Significant thermal degradation was observed in the DSC curve with broad intensity starting at 100 °C up to 300 °C. The exothermic peak at 300 °C can be attributed to the exothermic phenomenon caused by the thermal degradation of cellulose (Fan et al. 2016). Similar results were found by Li et al. (2021), who highlighted that small differences in exothermic peaks are due to the complex composition of the grape pomace that includes grape skins, fruit seeds, and stems, and a small number of oak chips.

Study of BSG dosage and effluent pH

The influence of the BSG adsorbent mass and the pH of the medium were investigated, and the results are shown in Fig. 5a and b, respectively. Figure 5a shows that the adsorption capacity of BSG decreased for both systems (Ni and Zn) when the adsorbent mass was increased from 0.0125 to 0.5 g. This negative effect of increasing the adsorbent dosage on the adsorption capacity occurs because, at higher dosages of BSG, the active adsorption sites remain unsaturated during the process (Rossato et al. 2020). Thus, studies of the effect of pH and adsorption kinetics for both nickel and zinc were evaluated using 0.0125 g of BSG.

The effect of pH on the adsorption capacity of Ni and Zn is shown in Fig. 5b. It can be seen that at basic pH, the adsorption capacities were more significant. This behavior occurs because, under acidic conditions, there is competition between the H^+ ions and the Ni and Zn ions for the adsorption sites. On the other hand, at alkaline pH, this competition decreases, and, therefore, adsorption occurs more easily (Peres et al. 2018). Therefore, all subsequent adsorption tests were carried out at pH 8, the actual pH of the effluent.

Kinetic results

The study of adsorption kinetics was observed through curves of adsorption capacity (q_t) versus time (t). The experimental kinetic data were fitted to pseudo-first-order (PFO) and pseudo-second-order (PSO) models. The results are presented in Fig. 6 and Table 2.

Based on Fig. 6, equilibrium time was reached around the first 60 min for both systems. At times above equilibrium, only a small variation in the maximum adsorption capacity was observed, indicating a possible saturation of the active sites of the BSG. Table 2 presents the values of the parameters found in the adjustments of the kinetic curves. High values of coefficient of determination ($R^2 > 0.97$) and low values of average relative error (ARE < 4.0) indicated that both models satisfactorily describe the adsorption kinetics.

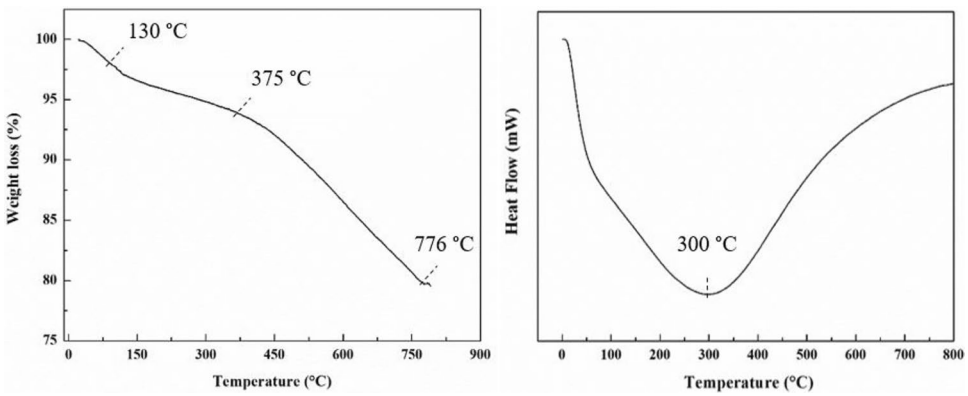

Fig. 4 TGA and DSC curves for BSG

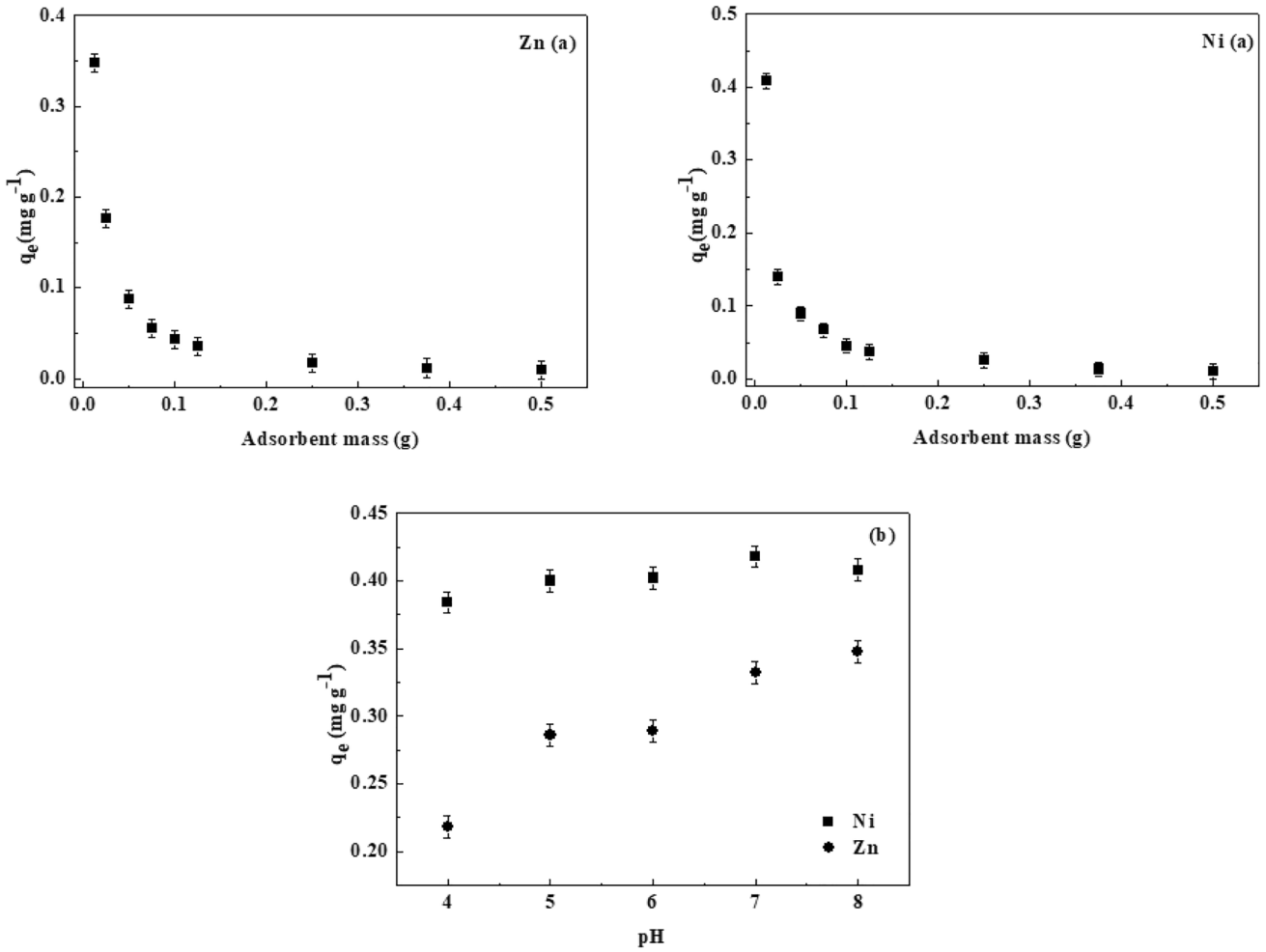

Fig. 5 Effects of BSG amount (**a**) and effluent pH (**b**) on the adsorption capacity of Zn and Ni

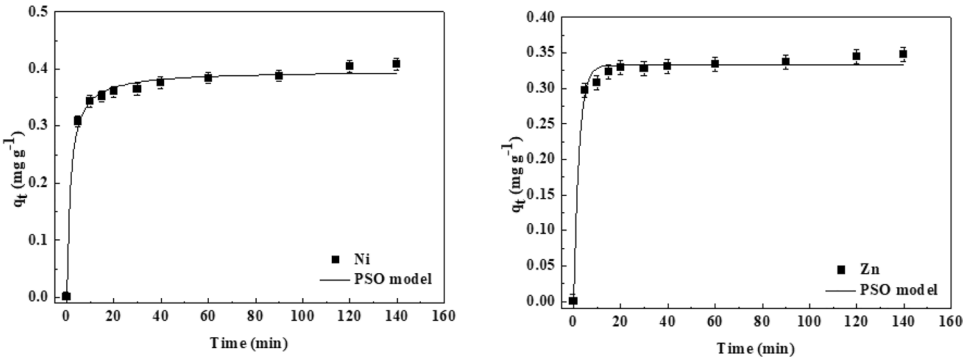

Fig. 6 Kinetic curves for the adsorption of Ni and Zn from the industrial effluent using BSG (T = 298 K, 200 rpm, V = 50 mL, pH = 8.0, and m = 0.0125 g)

Table 2 Kinetic parameters for the adsorption of Zn and Ni from the industrial effluent on the BSG

Metal	Kinetic models							
	PFO				PSO			
	q_1 (mg g^{-1})	k_1 (min^{-1})	R^2	*ARE* (%)	q_2 (mg g^{-1})	k_2 (g mg^{-1} min^{-1})	R^2	*ARE* (%)
Zn	0.332	0.423	0.9908	2.13	0.342	3.48×10^{-3}	0.9978	1.09
Ni	0.379	0.304	0.9765	3.83	0.397	1.56×10^{-3}	0.9942	1.83

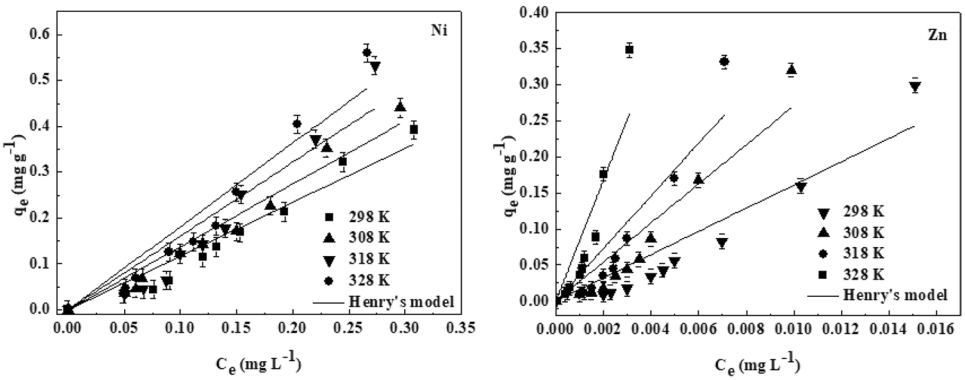

Fig. 7 Isotherm curves for the adsorption of Ni and Zn from the industrial effluent on the BSG (pH = 8.0, 200 rpm, and m = 0.25–10 g L^{-1})

Table 3 Equilibrium parameters for the adsorption of Ni and Zn on the BSG

	Henry's model	*T* (K)			
		298	308	318	328
Ni	k_H (L g^{-1})	1.17	1.37	1.61	1.82
	R^2	0.9473	0.9249	0.9579	0.8944
	ARE (%)	10.12	11.07	14.94	16.21
Zn	k_H (L g^{-1})	16.12	27.09	36.49	83.91
	R^2	0.8526	0.8581	0.8919	0.8894
	ARE (%)	12.08	10.83	15.78	20.65

Table 4 Thermodynamic parameters for the adsorption of Ni and Zn on the BSG

Material	*T* (K)	ΔG^0(kJ mol^{-1})	ΔH^0(kJ mol^{-1})	ΔS^0(kJmol^{-1} K^{-1})
Ni	298	−34.21	42.43	0.26
	308	−36.78		
	310	−39.35		
	328	−41.92		
Material	T (K)	ΔG^0(kJ mol^{-1})	ΔH^0(kJ mol^{-1})	ΔS^0 (kJmol^{-1} K^{-1})
Zn	298	−27.58	12.09	0.13
	308	−28.91		
	310	−30.24		
	328	−31.58		

Other parameters observed were the theoretical capacities (q_1 and q_2) which presented values very close to the experimental adsorption capacities, confirming the proper fit of the PFO and PSO models.

Equilibrium isotherms

The adsorption isotherms of Ni and Zn metals using BSG as adsorbent are shown in Fig. 7 and Table 3. According to the results, it is possible to observe similar behavior for both systems. Increasing the temperature from 298 to 328 K promoted an increase in the BSG adsorption capacity. Kayalvizhi et al. (2022) also reported that increased temperature facilitated Ni adsorption. The authors used an adsorbent based on biomaterial-activated sawdust–chitosan powder in this study. Jiang et al. (2021) studied the adsorption of Zn using a composite based on montmorillonite (MMT) and hummus-like substances (HLS) as adsorbents. They reported that in studies of adsorption isotherms, the increase in temperature favored the increase in the adsorption capacity, as in the present study.

The adsorption isotherms showed a linear behavior between concentration and adsorption capacity, typical for low adsorbate concentrations, as occurred in this study. So, the Henry model was chosen to represent the adjustment of the experimental data. The values of the coefficients of determination (R^2) (Table 3) for both systems were greater than 0.85, indicating an adequate fit to the data. Furthermore, Henry's constant (k_H) increased with increasing temperature, demonstrating that the affinity between BSG and Ni and Zn metals was greater at higher temperatures (Netto et al. 2019).

The adsorption of Ni and Zn metals in BSG achieved satisfactory results, as the initial concentration of contaminants was outside the standard limits for discarding the effluent in agricultural soil. Based on the requirements issued by the controlling agency, the liquid effluent must reach a maximum of 0.2 mg L^{-1} of nickel and 2.0 mg L^{-1} of zinc. Both metals were successfully removed from the real effluent, presenting final concentration values within the limit allowed by legislation. In addition, it is necessary to emphasize the use of an adsorbent developed from a natural precursor (grape pomace) with very interesting properties in adsorption.

Thermodynamics results

The thermodynamic adsorption parameters ΔG^0, ΔS^0, and ΔH^0 (Table 4) were obtained from the equilibrium constant of the Henry model (k_H) used in the adsorption isotherms. The parameters were calculated according to Lima et al. (2019).

Based on Table 4, negative values of ΔG^0 indicate that the adsorption process was favorable and spontaneous. As for ΔH^0, positive values indicated an endothermic process, confirming that adsorption was favored at higher temperatures. Positive values were also verified for ΔS^0, demonstrating that the perturbation of the system at the solid–liquid interface increased during adsorption (Georgin et al. 2021).

Possible adsorption interactions

A possible mechanism was proposed based on the pH effect results (Fig. 5), thermodynamic parameters (Table 4), and FTIR analyses before and after adsorption (not shown). Firstly, at pH 8, the BSG is negatively charged due to the deprotonation of oxygenated groups (OH, COOH) (Streit et al. 2021; Silva et al. 2021). The metals are cations or hydrated cations. Consequently, electrostatic interactions could occur. This type of interaction is supported by the pH effect and by the spectrum of BSG after adsorption, where the bands around 3400 (OH) and 1070 (CO) shifted. Besides, the magnitude of ΔH^0 for Ni is of electrostatic forces (Dotto et al. 2011). Secondly, ΔS^0 was positive for both metals, indicating rearrangements of water molecules on the BSG surface. The magnitude of ΔH^0 for Zn is of H-bonds. Finally, we can support that H-bonds and electrostatic forces were involved in the Ni and Zn adsorption on the BSG.

Conclusion

Biochar from Serra Gaúcha (BSG) derived from grape pomace, a residue from the wine industry, was prepared and used to remove Ni and Zn metals from the real effluent of a local company originating from the pre-treatment and painting process. BSG had relevant functional groups, a positive physical structure in the adsorption process, and confirmed the material's mesoporosity. In addition, the use of adsorption with BSG was effective in polishing the effluent, since the removal of metals reached satisfactory levels, below the standard required by current legislation. Finally, the proposed treatment requires low amounts of BSG short time (60 min) and could be carried out without pH adjustment.

Supplementary Information The online version contains supplementary material available at https://doi.org/10.1007/s11356-022-20488-4.

Author contribution Conceptualization, F. L. Carvalho, F. Ketzer, and G. L. Dotto; methodology, R. R. Schio and J. P. dos Santos; formal analysis and investigation, R. R. Schio and J. P. dos Santos; writing — original draft preparation, F. L. Carvalho, F. Ketzer, R. R. Schio, and J. P. dos Santos; writing — review and editing, G. L. Dotto, D. Pinto, and L. F. O. Silva; funding acquisition, G. L. Dotto and L. F. O. Silva; and supervision, G. L. Dotto. All authors read and approved the final manuscript.

Funding The authors would like to thank Coordination for the Improvement of Higher Education Personnel (CAPES) and National Council for Scientific and Technological Development (CNPq) for their financial support.

Data availability The datasets used and analyzed during the current study are available from the corresponding author on reasonable request.

Declarations

Ethics approval Not applicable.

Consent to participate Not applicable.

Consent for publication Not applicable.

Competing interests The authors declare no competing interests.

References

Ahmad M, Lee SS, Dou X, Mohan D, Sung J-K, Yang JE, Ok YS (2012) Effects of pyrolysis temperature on soybean stover- and peanut shell-derived biochar properties and TCE adsorption in water. Bioresour Technol 118:536–544. https://doi.org/10.1016/j.biortech.2012.05.042

Al-Lagtah NMA, Al-Muhtaseb AH, Ahmad MNM, Salameh Y (2016) Chemical and physical characteristics of optimal synthesized activated carbons from grass-derived sulfonated lignin versus commercial activated carbon. Micropor Mesopor Mat 225:504–514. https://doi.org/10.1016/j.micromeso.2016.01.043

Anirudhan TS, Sreekumari SS (2011) Adsorptive removal of heavy metal ions from industrial effluents using activated carbon derived from waste coconut buttons. J Environ Sci (china) 23:1989–1998. https://doi.org/10.1016/S1001-0742(10)60515-3

Bilal M, Shah JA, Ashfaq T, Gardazi SMH, Tahir AA, Pervez A, Haroon H, Mahmood Q (2013) Waste biomass adsorbents for copper removal from industrial wastewater—a review. J Hazard Mater 263:322–333. https://doi.org/10.1016/j.jhazmat.2013.07.071

Bonilla-Petriciolet, A., Mendoza-Castillo, D.I., Dotto, G.L., Duran-Valle, C.J. 2019. 1 ed. Adsorption in water treatment. Reference module in chemistry, molecular sciences and chemical engineering 1 Elsevier, Amsterdam, pp. 1–21. https://doi.org/10.1016/B978-0-12-409547-2.14390-2

Brezoiu AM, Matei C, Deaconu M, Stanciuc AM, Trifan A, Pintiliescu AG, Berger D (2019) Polyphenols extract from grape pomace. Characterization and valorisation through encapsulation into mesoporous silica-type matrices. Food Chem Toxicol 133:110787. https://doi.org/10.1016/j.fct.2019.110787

Cao X, Harris W (2010) Properties of dairy-manure-derived biochar pertinent to its potential use in remediation. Bioresour Technol 101:5222–5228. https://doi.org/10.1016/j.biortech.2010.02.052

Cao X, Ma L, Liang Y, Gao B, Harris W (2011) Simultaneous immobilization of lead and atrazine in contaminated soils using dairy-manure biochar. Environ Sci Technol 45:4884–4889. https://doi.org/10.1021/es103752u

Casazza AA, Aliakbarian B, Lagazzo A, Garbarino G, Carnasciali MM, Perego P, Busca G (2016) Pyrolysis of grape marc before and after the recovery of polyphenol fraction. Fuel Process Technol 153:121–128. https://doi.org/10.1016/j.fuproc.2016.07.014

Dil EA, Ghaedi M, Asfaram A, Mehrabi F, Sadeghfar F (2019) Efficient adsorption of azure B onto CNTs/Zn:ZnO@Ni2P-NCs from

aqueous solution in the presence of ultrasound wave based on multivariate optimization. J Ind Eng Chem 74:55–62. https://doi.org/10.1016/j.jiec.2018.12.050

Dotto GL, McKay G (2020) Current scenario and challenges in adsorption for water treatment. J Environ Chem Eng 8:103988. https://doi.org/10.1016/j.jece.2020.103988

Dotto, G.L., Salau, N.P.G., Piccin, J.S., Cadaval Jr., T.R.S., Pinto, L.A.A. 2017. Adsorption kinetics in liquid phase: modeling for discontinuous and continuous systems, Chapter 3, In: A. Bonilla-Petriciolet, D.I. Mendoza-Castillo, H.E. Reynel-Ávila (Eds.), Adsorption processes for water treatment and purification, Springer International Publishing. https://doi.org/10.1007/978-3-319-58136-1_3

Dotto GL, Vieira MLG, Gonçalves JO, Pinto LAA (2011) Removal of acid blue 9, food yellow 3 and fd&c yellow n° 5 dyes from aqueous solutions using activated carbon, activated earth, diatomaceous earth, chitin and chitosan: equilibrium studies and thermodynamic. Quím Nova 34:1193–1199. https://doi.org/10.1590/s0100-40422011000700017

Fan X, Gao Y, He W, Hu H, Tian M, Wang K, Pan S (2016) Production of nano bacterial cellulose from beverage industrial waste of citrus peel and pomace using *Komagataeibacter xylinus*. Carbohydr Polym 151:1068–1072. https://doi.org/10.1016/j.carbpol.2016.06.062

Ferrari V, Taffarel SR, Espinosa-Fuentes E, Oliveira MLS, Saikia BK, Silva LFO (2019) Chemical evaluation of by-products of the grape industry as potential agricultural fertilizers. J Clean Prod 208:297–306. https://doi.org/10.1016/j.jclepro.2018.10.032

Georgin J, de Salomón YIO, Franco DSP, Netto MS, Piccilli DGA, Perondi D, Silva LFO, Foletto EL, Dotto GL (2021) Development of highly porous activated carbon from Jacaranda mimosifolia seed pods for remarkable removal of aqueous-phase ketoprofen. J Environ Chem Eng 9:105676. https://doi.org/10.1016/j.jece.2021.105676

González-García P (2018) Activated carbon from lignocellulosics precursors: a review of the synthesis methods, characterization techniques and applications. Renew Sust Energ Rev 82:1393–1414. https://doi.org/10.1016/j.rser.2017.04.117

Gope, M., Saha, R. 2021. Removal of heavy metals from industrial effluents by using biochar, Intelligent Environmental Data Monitoring for Pollution Management, p. 25–48. https://doi.org/10.1016/B978-0-12-819671-7.00002-6.

Jiang K, Liu K, Peng Q, Zhou M (2021) Adsorption of Pb(II) and Zn(II) ions on humus-like substances modified montmorillonite. Colloids Surf, A Physicochem Eng Asp 631:127706. https://doi.org/10.1016/j.colsurfa.2021.127706

Kayalvizhi K, Alhaji NMI, Saravanakkumar D, Mohamed SB, Kaviyarasu K, Ayeshamariam A, Al-Mohaimeed AM, AbdelGawwad MR, Elshikh MS (2022) Adsorption of copper and nickel by using sawdust chitosan nanocomposite beads A kinetic and thermodynamic study. Environ Res 203:111814. https://doi.org/10.1016/j.envres.2021.111814

Li H, Xiong J, Xiao T, Long J, Wang Q, Li K, Liu X, Zhang G, Zhang H (2019) Biochar derived from watermelon rinds as regenerable adsorbent for efficient removal of thallium(I) from wastewater. Process Saf Environ Prot 257–266. https://doi.org/10.1016/j.psep.2019.04.031

Li ZY, Azi F, Dong JJ, Liu LZ, Ge ZW, Dong MS (2021) Green and efficient in-situ biosynthesis of antioxidant and antibacterial bacterial cellulose using wine pomace. Int J Biol Macromol. https://doi.org/10.1016/j.ijbiomac.2021.11.049.

Lima EC, Hosseini-Bandegharaei A, Moreno-Piraján JC, Anastopoulos I (2019) A critical review of the estimation of the thermodynamic parameters on adsorption equilibria. Wrong use of equilibrium constant in the Van't Hoof equation for calculation of thermodynamic parameters of adsorption. J Mol Liq 273:425–434. https://doi.org/10.1016/j.molliq.2018.10.048

Lütke SF, Igansi AV, Pegoraro L, Dotto GL, Pinto LAA, Cadaval Jr TRS (2019) Preparation of activated carbon from black wattle bark waste and its application for phenol adsorption. J Environ Chem Eng 7:103396. https://doi.org/10.1016/j.jece:2019.103396

Mulinari DR, Voorwald HJC, Cioffi MO, Silva MLCP, Luz SM (2009) Preparation and properties of HDPE/sugarcane bagasse cellulose composites obtained for thermokinetic mixer. Carbohydr Polym 75:317–321. https://doi.org/10.1016/j.carbpol.2008.07.028

Netto MS, Rossato DL, Jahn SL, Mallmann ES, Dotto GL, Foletto EL 2019 Preparation of a novel magnetic geopolymer/zero–valent iron composite with remarkable adsorption performance towards aqueous Acid Red 97. Chem Eng Commun 1048-1061. https://doi.org/10.1080/00986445.2019.1635467

Oncel MS, Muhcu A, Demirbas E, Kobya M (2013) A comparative study of chemical precipitation and electrocoagulation for treatment of coal acid drainage wastewater. J Environ Chem Eng 1:989–995. https://doi.org/10.1016/j.jece.2013.08.008

Peng L, Bartzas G 2021 Heavy metals and metalloids: a serious threat to environment and human health. Curr Opin Environ Sci Health Editorial overview, 23, Article 100287. https://doi.org/10.1016/j.coesh.2021.100287.

Peres EC, Cunha JM, Dortzbacher GF, Pavan FA, Lima EC, Foletto EL, Dotto GL (2018) Treatment of leachates containing cobalt by adsorption on Spirulina sp. and activated charcoal. J Environ Chem Eng 6:677–685. https://doi.org/10.1016/j.jece.2017.12.060

Piccin JS, Cadaval Jr., TRS, Pinto LAA, Dotto GL 2017 Adsorption isotherms in liquid phase: experimental, modeling, and interpretations, Chapter 2, in: A. Bonilla-Petriciolet, D.I. Mendoza-Castillo, H.E. Reynel-Ávila (Eds.), Adsorption processes for water treatment and purification, Springer International Publishing. Adsorption. https://doi.org/10.1007/978-3-319-58136-1_2

Pigatto RS, Franco DSP, Netto MS, Carissimi É, Oliveira LFS, Jahn SL, Dotto GL 2020 An eco-friendly and low-cost strategy for groundwater defluorination: adsorption of fluoride onto calcinated sludge. J Environ Chem Eng Article 104546. https://doi.org/10.1016/j.jece.2020.104546

Rathi BS, Kumar PS 2021 Application of adsorption process for effective removal of emerging contaminants from water and wastewater. Environ Pollut 280, Article 116995. https://doi.org/10.1016/j.envpol.2021.116995.

Rosa SMC, Nossol ABS, Nossol E, Zarbin AJG, Zamora PGP 2017 Non-synergistic UV-A photocatalytic degradation of estrogens by nano-TiO2 supported on activated carbon. J Braz Chem Soc 28.https://doi.org/10.5935/0103-5053.20160201

Rossato DL, Netto MS, Jahn SL, Mallman ES, Dotto GL, Foletto EL (2020) Highly efficient adsorption performance of a novel magnetic geopolymer/Fe3O4 composite towards removal of aqueous acid green 16 dye. J Environ Chem Eng 8:103804. https://doi.org/10.1016/j.jece.2020.103804

Roy A, Bharadvaja N (2021) Efficient removal of heavy metals from artificial wastewater using biochar. Environ Nanotechnol Monit Manag. https://doi.org/10.1016/j.enmm.2021.100602

Santos DCD, Adebayo MA, Lima EC, Pereira SFP, Cataluña R, Saucier C, Thue PS, Machado FM (2015) Application of carbon composite adsorbents prepared from coffee waste and clay for the removal of reactive dyes from aqueous solutions. J Braz Chem Soc 26:924–938. https://doi.org/10.5935/0103-5053.20150053

Sardella F, Gimenez M, Navas C, Morandi C, Deiana C, Sapang K (2015) Conversion of viticultural industry wastes into activated carbons for removal of lead and cadmium. J Environ Chem Eng 3:253–260. https://doi.org/10.1016/j.jece.2014.06.026

Shao L, Ren Z, Zhang G, Chen L (2012) Facile synthesis, characterization of a MnFe 2O 4/activated carbon magnetic composite

and its effectiveness in tetracycline removal. Mater Chem Phys 135:16–24. https://doi.org/10.1016/j.matchemphys.2012.03.035

Silva NF, Netto MS, Silva LFO, Mallmann ES, Lima EC, Ferrari V, Dotto GL (2021) Composite carbon materials from winery composted waste for the treatment of effluents contaminated with ketoprofen and 2-nitrophenol. J Environ Chem Eng 9:105421. https://doi.org/10.1016/j.jece.2021.105421

Sing KSW, Everett DH, Haul RAW, Moscou L, Pieroti RA, Rouquerol J, Siemieniewska T (1985) Reporting physisorption data for gas/solid systems with special reference to the determination of surface area and porosity. Pure Appl Chem 57:603–619. https://doi.org/10.1351/pac198557040603

Streit AFM, Collazzo GC, Druzian SP, Verdi RS, Foletto EL, Oliveira LFS, Dotto GL (2021) Adsorption of ibuprofen, ketoprofen, and paracetamol onto activated carbon prepared from effluent treatment plant sludge of the beverage industry. Chemosphere 262:128322. https://doi.org/10.1016/j.chemosphere.2020.128322

Tang SH, Ahmad Zaini MA (2020) Development of activated carbon pellets using a facile low-cost binder for effective malachite green dye removal. J Cleaner Prod 253:119970. https://doi.org/10.1016/j.jclepro.2020.119970

Tareq R, Akter N, Azam MDS 2019 Biochars and biochar composites: low-cost adsorbents for environmental remediation. Biochar Biomass Waste 169-209. https://doi.org/10.1016/B978-0-12-811729-3.00010-8

Vilvanathan S, Shanthakumar S 2015 Biosorption of Co(II) ions from aqueous solution using Chrysanthemum indicum: kinetics, equilibrium and thermodynamics, Process Saf Environ Prot 98-110. https://doi.org/10.1016/j.psep.2015.05.001

Yang Q, Meng X, Zhao H, Cao C, Liu Y, Huisingh D (2021) Sustainable operations-oriented painting process optimisation in automobile maintenance service. J Clean Prod 324:129191. https://doi.org/10.1016/j.jclepro.2021.129191

Zhou G, Liu C, Chu L, Tang Y, Luo S (2016) Rapid and efficient treatment of wastewater with high-concentration heavy metals using a new type of hydrogel-based adsorption process. Bioresour Technol 219:451–457. https://doi.org/10.1016/j.biortech.2016.07.038

Publisher's note Springer Nature remains neutral with regard to jurisdictional claims in published maps and institutional affiliations.